

Full length article

# Revealing the nonlinear dynamics of VCSEL-based frequency combs induced by optical injection

Daniel Plaza-Vas<sup>a,b,c</sup>, Angel Valle<sup>c</sup>, Nathalie Vermeulen<sup>a</sup>, Ana Quirce<sup>a,c,\*</sup><sup>a</sup> Brussels Photonics (B-PHOT), Department of Applied Physics and Photonics, Vrije Universiteit Brussel (VUB), Pleinlaan 2, Brussels, 1050, Belgium<sup>b</sup> Departamento de Física Moderna, Universidad de Cantabria (UC), Avda. Los Castros s/n, Santander, 39005, Spain<sup>c</sup> Instituto de Física de Cantabria (IFCA), Universidad de Cantabria-CSIC, Avda. Los Castros s/n, Santander, 39005, Spain

## ARTICLE INFO

## Keywords:

Semiconductor lasers  
VCSELS  
Optical frequency combs  
Optical injection  
Gain-switching  
Nonlinear dynamics

## ABSTRACT

Optical injection (OI) into VCSELS is a powerful tool to control VCSEL behavior and light emission. Previous studies by Doumbia et al. 2021 have shown that OI of a 3-line optical frequency comb (OFC) into a VCSEL allows tailoring the properties of the OFCs emitted in the VCSEL output light. Our efforts extend beyond the previous findings, as for the first time, we study the polarization-resolved nonlinear dynamics maps found in a VCSEL subject to two different types of orthogonal OI, namely continuous-wave (CW) injection and the injection of a 3-line gain-switched (GS) OFC. Our results reveal that, within a significant parameter region (encompassing frequency detuning and injected power), the VCSEL's nonlinear behaviors induced by the OI of a GS-OFC are mainly determined by two factors: (1) the frequencies of the nonlinear dynamics of the VCSEL under CW OI, and (2) the polarization switching curves obtained under both types of OI. Therefore, (1) and (2) provide guidelines to understand the OFCs obtained at the output of the VCSEL. When injecting a 3-line OFC with 2 GHz frequency comb spacing, we demonstrate OFCs with approximately 50 GHz width at the output of the VCSEL, similar to the experimental results of Doumbia et al. 2021. We also identify the nonlinear dynamics that underpin these results.

## 1. Introduction

The development of optical frequency combs (OFCs) has witnessed great progress over the past decades. An OFC consists of a series of evenly spaced and highly coherent spectral components. In the time domain, these evenly spaced spectral components correspond to a pulse train, with a repetition rate equal to the frequency spacing ( $\Delta f'$ ) between the spectral components. OFCs find applications in different fields such as metrology, high-precision spectroscopy, high-speed optical communications, optical ranging, and (sub-)THz-wave generation [1–6]. OFCs can be generated by, amongst others, edge-emitting semiconductor lasers such as Distributed Feedback Lasers (DFB) [7,8], Discrete Mode Lasers (DML) [5,9] and Vertical-Cavity Surface-Emitting Lasers (VCSELS) [10]. In this work, we study OFC generation in VCSELS.

VCSELS have been widely investigated since the late 1970s due to their inherent advantages such as single longitudinal mode operation, emission wavelength tunability, low threshold current, high-speed modulation, low power consumption, reduced manufacturing costs, mass production and great compactness [11,12]. Single-mode VCSELS can emit linearly polarized light along one of two orthogonal directions due to cavity anisotropies [12]. Understanding and controlling the

polarization of VCSELS is also important in the frame of OFC generation. Several techniques can be used to produce OFCs, for example, modulators based on the electro-optic effect such as Mach Zehnder modulators (MZM) [13–15], mode-locking (ML) [16], or gain switching (GS) [7,9,10,17–20]. GS is used to create a regular pulse train at the output of a semiconductor laser and requires applying a periodic, generally sinusoidal, radiofrequency (RF) large signal modulation superimposed on a direct bias current. It is an easy-to-implement and low-cost technique that offers good correlation between optical modes, flexibility in the selection of the OFC repetition rate, and large central wavelength tunability [7,9,10,17–20]. The bias current applied to the laser, the modulation frequency  $f_{mod}$  and the modulation amplitude ( $V_{RF}$ ) are key parameters to tailor the spectral characteristics of the GS-OFCs [19,20].

The generation of GS-OFCs has been successfully demonstrated in edge-emitting lasers [7,20] and VCSELS [10,21,22]. When exploiting both linear polarizations present in VCSELS, it has been shown both experimentally [10] and theoretically [22] that the GS technique generates two orthogonally polarized combs that, combined, produce a wider overall comb. Dual-polarization VCSEL-based OFC generators

\* Corresponding author at: Instituto de Física de Cantabria (IFCA), Universidad de Cantabria-CSIC, Avda. Los Castros s/n, Santander, 39005, Spain.  
E-mail address: [quirce@ifca.unican.es](mailto:quirce@ifca.unican.es) (A. Quirce).

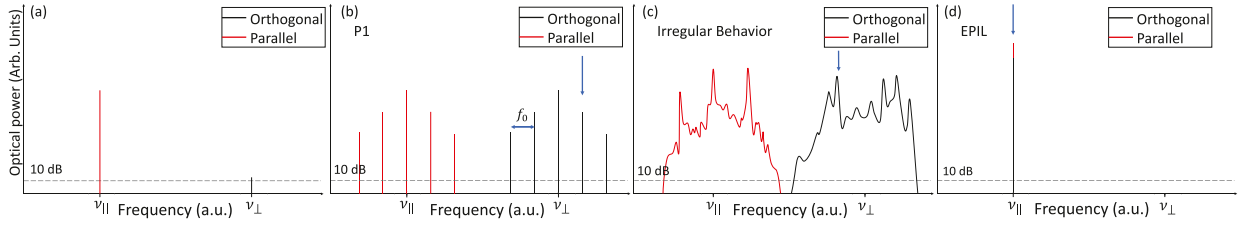


**Fig. 1.** (a) Schematic optical spectrum of the free-running VCSEL. (b–d) Schematic optical spectra corresponding to different nonlinear dynamics observed in a VCSEL under orthogonal CW OI: (b) P1 dynamics in both polarizations, (c) irregular behavior in both polarizations, and (d) EPIL, which stands for elliptically polarized injection locking. The parallel polarization is depicted in red, the orthogonal polarization in black, and injection frequencies are indicated by blue arrows. Spectra in Fig. 1(b–d) are represented for arbitrary frequency detunings and arbitrary power injections. The dashed horizontal line in the optical spectra represents 10 dB above the noise level.

can be used for polarization sensitive sensing, polarization-division multiplexing, and other polarization-dependent applications [10].

Whereas GS-OFCs benefit from the inherent advantages of the GS technique as outlined above, they typically only have a limited number of comb lines, large temporal jitter and chirp, and poor carrier-to-noise ratio. One approach to improve their characteristics and to expand the comb bandwidth is by means of Optical Injection (OI). OI is a technique that is often applied to VCSELs to improve their performance and explore their nonlinear dynamics [23–29]. For example, Continuous Wave (CW) OI into VCSELs has already been extensively studied and is known to induce polarization switching (PS) [25,30–32], establish nonlinear dynamics and, in general, allows exploiting the polarization properties of VCSELs [24,26,29]. In this work, we study OI in combination with OFC generation.

An OFC can be injected into a laser with CW operation to broaden the injected OFC bandwidth. The injection of a modulated signal into edge-emitting lasers has recently been investigated [15,33–37]. OFC expansion has been demonstrated by varying the injection parameters (frequency detuning and injected power ( $P_{inj}$ )) and the injected comb properties (frequency spacing and amplitude of the injected comb) [15,37]. In addition, in [34,35] the authors have demonstrated the possibility of generating sub-harmonic OFCs from the injected one.

The approach of OFC injection has been investigated to a lesser extent in VCSELs [14,38]. A few recent works have studied the nonlinear dynamics of VCSELs under the injection of a 3-line OFC [14,38] generated by a MZM, with parallel [38] and orthogonal polarization to that of the free-running VCSEL [14,38]. Dombia et al. have shown that by customizing and controlling the optical injection parameters it is possible to tailor the properties of the OFCs of the VCSEL output light. Under certain injection conditions, the competition of polarization modes can induce either a single-polarization OFC or a dual-polarization OFC (both polarizations of the VCSEL are excited). The latter case, under orthogonal OI, has proved to be the most favorable scenario for extending the bandwidth of the 3-line injected comb and for improving its characteristics such as carrier-to-noise ratio (CNR) [14,38]. In [14] the optimization of the injection parameters has demonstrated dual-polarization OFCs at the output of the VCSEL with a bandwidth of 60 GHz for a comb spacing of 2 GHz and a CNR of up to 60 dB.

However, no systematic study of the nonlinear dynamics of the system was carried out in these previous studies [14,38]. In this work, we present, for the first time, a systematic analysis of polarization-resolved nonlinear dynamics maps under both CW injection and 3-lines OFC injection in a single-mode VCSEL. This analysis spans the frequency range covered by both polarizations of the free-running VCSEL. In both injection cases, the injection is done in orthogonal polarization to the polarization of the free-running VCSEL.

In our study, the injection is carried out using a GS-OFC. Our results show that within a significant parameter region – encompassing frequency detuning and injected power – the VCSEL’s nonlinear behaviors induced by the OI of a 3-line GS-OFC are dictated by two factors. The first is the frequencies of the nonlinear dynamics of the VCSEL under CW OI, and the second is the PS curves obtained under CW OI and

when injecting a GS-OFC. Therefore, the CW nonlinear dynamics map and the PS curves as presented in this work, provide a useful guide to reveal the nonlinear dynamics of the OFCs obtained at the VCSEL’s output.

Our paper is organized as follows: Section 2 explains the basic concepts of OI in VCSELs. In Section 3 we describe the experimental setup. Section 4.1 presents the polarization resolved nonlinear dynamics maps under both CW and GS-OFC injection. Section 4.2 provides optical spectra with relevant examples of nonlinear dynamics identified in Section 4.1. Section 4.3 shows the overlaid contours of the regions of nonlinear dynamics maps for both CW injection and frequency comb injection. Section 4.4 analyzes the mapping of the fundamental oscillation frequency and the optical spectral width of the periodic dynamics found in the VCSEL under CW injection. Finally, in Section 5, discussion and conclusions are presented.

## 2. Basic concepts of optical injection in VCSELs

Semiconductor lasers, and in particular VCSELs, due to their linewidth enhancement factor, can be either stabilized or destabilized through external perturbations such as CW [24–29,32] or modulated optical injection [14,38], leading to a variety of nonlinear dynamics.

Optical injection consists of injecting light from an external master laser into a slave laser (in our work, a VCSEL) [26–29]. Depending on the polarization of the injected beam, two different injection schemes can be considered: parallel or orthogonal OI. In the case of parallel OI, linearly polarized light is injected parallel to the dominant polarization of the free-running VCSEL [27]. With orthogonal OI, linearly polarized light is injected perpendicular to the one of the free-running VCSEL [26–28].

### 2.1. Continuous-wave optical injection

Throughout this section, we describe the fundamental concepts of CW OI. In this case, light from an external master laser operating in a continuous-wave regime is injected into the VCSEL. The frequency detuning,  $\Delta\nu$  (defined as the frequency difference between the master and the slave laser), the injected power from the master to the slave laser,  $P_{inj}$ , and the polarization direction of the injected beam, are the key parameters that play a crucial role in the dynamics observed in the VCSEL.

To visually demonstrate these dynamics, Fig. 1 displays various optical spectrum diagrams, each representing different dynamic states. These spectra representations depict situations of arbitrary frequency detuning and arbitrary power injection. Orthogonal and parallel polarizations of the VCSEL are represented in black and red, respectively, while the injection frequencies are indicated by blue arrows. This color representation will be consistently used across the remaining text.

Single-mode VCSELs inherently display two polarization modes that correspond to the two orthogonal polarizations of the device’s fundamental transverse mode. This characteristic emerges from polarization anisotropies introduced during the fabrication process. These

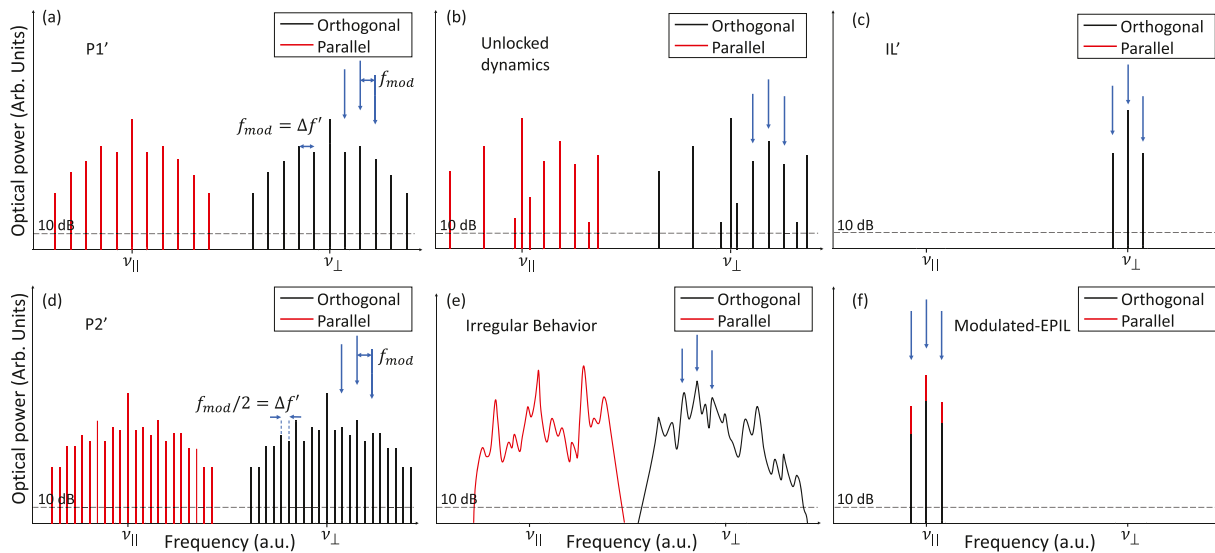


**Fig. 2.** Schematic optical spectra corresponding to different nonlinear dynamics observed in a VCSEL under orthogonal OFC injection: (a) P1' in both polarizations, (b) unlocked dynamics, (c) IL', (d) P2' in both polarizations, (e) irregular behavior in both polarizations, and (f) modulated-EPIL. The parallel polarization is depicted in red, the orthogonal polarization in black, and injection frequencies are indicated with blue arrows. Spectra in Fig. 2(a)–(f) are represented for arbitrary frequency detunings and arbitrary power injections. The dashed horizontal line in the optical spectra represents 10 dB above the noise level.

modes have distinct wavelengths and given the VCSEL's wavelength-dependent gain spectrum, each mode will have a different gain value, which leads to the preferential amplification of one mode over its counterpart [12]. Fig. 1(a) presents the optical spectrum diagram for the free-running VCSEL under conditions of an arbitrary bias current and temperature. In this state, the VCSEL emits in the dominant, or “parallel” polarization, denoted by  $\nu_{\parallel}$ , while the orthogonal polarization, represented by  $\nu_{\perp}$ , is suppressed.

Continuous-wave orthogonal OI has been demonstrated to induce rich nonlinear dynamics, including injection locking (IL), periodic dynamics and chaos [26–28], and new features, such as elliptically polarized injection-locked states (EPIL) [39] which are not observed under parallel OI.

IL refers to a steady state where the slave laser is locked to the frequency, phase, and polarization of the master laser [23]. When an external optical signal is injected into a laser, particularly a VCSEL, it interacts with the photons within the laser cavity, modulating the carriers in the active region. This interaction is governed by rate equations that account for the dynamics between the injected photons, the intracavity photons of the slave laser, the carriers, and the phase difference between the slave and injected fields. The injection process induces changes in the slave laser's frequency through two mechanisms: the shift in resonance due to variations in carrier density and the coupling between the injected and internal fields. As the optical injection amplifies stimulated emission in the active region, it induces a reduction in carrier density and an increase of the refractive index, influencing the rate of carrier recombination and photon emission. Consequently, the natural lasing frequency of the VCSEL might gradually synchronize with the frequency of the external signal. When the accumulated frequency shifts match the difference in frequency between the master and slave lasers, the slave laser reaches an injection-locked state. Due to the continuous phase shift introduced by the injected light, the output aligns with the master laser's frequency, producing light that is locked to the frequency, phase, and polarization of the master laser. The efficiency and range of this locking phenomenon is influenced by factors such as detuning, injection strength, and the linewidth enhancement factor [40]. IL has attracted much interest as it allows improving the semiconductor laser characteristics without modifying its design. For instance, it can be used to reduce the laser linewidth and the frequency chirp, or to enhance the modulation bandwidth [23].

Outside the locking region, the stationary locked state evolves to more complex dynamics due to the nonlinear interaction between the electric fields of the injected light and the VCSEL. The resulting complex dynamics includes periodic dynamics, wave-mixing or even irregular behaviors. Periodic behavior can appear at a frequency that results from the beating between the optical injection and the slave electric fields. Limit cycles, also known as Period 1 (P1), represent stable, periodic oscillations. In the context of our work, we use  $f_0$  to denote the oscillation frequency of the P1 dynamic. There is also the occurrence of period doubling, termed as Period 2 (P2), when oscillations manifest at half of the frequency of the P1. Both of these phenomena have been previously observed and documented [27–29]. In general, periodic dynamics can appear in either the parallel, the orthogonal, or both polarizations of the VCSEL. We identify P1 dynamics in a particular polarization by measuring its optical spectrum. When new side peaks equally spaced in frequency at 10 dB above the noise level, develop around the VCSEL's orthogonal and/or parallel polarization, we classify the P1 as present in the respective polarization. Fig. 1(b) illustrates a generic optical spectrum diagram corresponding to P1 dynamics in both polarizations of the VCSEL. Fig. 1(b) shows that as a result of continuous-wave injection, equidistant peaks in frequency develop around the parallel and orthogonal polarization of the VCSEL, leading to the presence of P1 dynamics in both polarizations. In the case illustrated in Fig. 1(b), the spectral components of both polarizations are equally separated by the same P1 oscillation frequency,  $f_0$ .

The output of the VCSEL can also be destabilized leading to irregular oscillations or chaos. The chaotic regime is characterized by a broad and noisy optical spectrum without well-defined frequencies [28]. An example of irregular behavior in both polarizations is illustrated in Fig. 1(c). Alternatively, the interaction between the injected light field and the VCSEL's intrinsic lasing field – influenced by factors like injection strength, frequency detuning, the operational temperature of the VCSEL, bias current, and intrinsic properties of the device – may result in a redistribution of gain between the two orthogonal polarization modes of the VCSEL leading to PS [30,31,41]. PS refers to the situation in which the output of the VCSEL changes from the polarization with the higher gain to the weaker polarization. We say that PS to the orthogonal polarization of the VCSEL takes place when the power ratio between the two polarizations is greater than 20 dB in favor of the orthogonal one.

When CW orthogonal OI is close to the parallel polarization of the free-running VCSEL, a stationary EPIL state was theoretically predicted in [32] using the Spin-Flip Model, and later experimentally verified in [39]. EPIL refers to a two-mode injection-locked solution where both polarizations of the slave laser are excited, and frequency locked to the master laser [24,32,39] (see Fig. 1(d)). The emergence and stability limits of the EPIL solution are significantly influenced by the spin-flip relaxation rate of the VCSEL. An in-depth analysis of the bifurcation leading to this solution can be found in [32].

The nonlinear dynamics under CW injection will be important to explain the experimental results later on.

## 2.2. OFC injection

In this section, we describe the fundamental concepts of optical injection when an OFC from an external master laser is injected orthogonal to the parallel polarization of the free-running VCSEL. For simplicity, our discussion will center on the injection of a three-line OFC, which aligns with our experimental approach. While the principles and explanations provided here could be extrapolated to the injection of an OFC with more lines, our study began by focusing on the most straightforward choice: a three-line comb configuration. However, the principles and explanations provided here could be extrapolated to the injection of an OFC with more lines. As mentioned earlier, under CW OI,  $\Delta\nu$ ,  $P_{inj}$ , and the polarization direction of the injected beam are parameters that play a key role in the nonlinear dynamics observed in the VCSEL. Under modulated injection, the parameters of the injected comb, i.e., modulation frequency ( $f_{mod}$ ) and modulation amplitude ( $V_{RF}$ ), also become essential. We use the apostrophe notation in the context of injection locking (IL') and periodic combs achieved through OFC injection to distinguish it from the dynamics arising from CW injection.

A periodic comb,  $PN'$ , is defined as a dynamical state in which the optical frequency comb, in the corresponding polarization, has a frequency spacing of  $\Delta f' = f_{mod}/N'$  between consecutive lines in its optical spectrum, with  $N'$  being a natural number. We term  $\Delta f'$  as the frequency spacing of the OFC at the output of the VCSEL, resulting from OFC injection. Moreover, to consider a  $PN'$  comb, additional spectral lines relative to the injected comb must appear in the optical spectrum of the corresponding VCSEL polarization (in our case, this involves more than three lines), with an amplitude of at least 10 dB above the noise level. Fig. 2 presents several optical spectrum diagrams, each corresponding to different nonlinear dynamic states under the injection of a three-line OFC with an arbitrary modulation frequency,  $f_{mod}$ , amplitude modulation, frequency detuning, and injected power. Fig. 2(a) and (d) depict a  $P1'$  comb with 11 teeth and a  $P2'$  comb with 22 teeth in both polarizations, respectively. In the  $P1'$  comb, the frequency spacing between the comb lines equals the modulation frequency, i.e.  $\Delta f' = f_{mod}$  as  $N' = 1$ , while in the  $P2'$  comb, the frequency spacing is half the modulation frequency  $\Delta f' = f_{mod}/2$ .

Unlocked dynamics and irregular behavior in the parallel and/or in the orthogonal polarization, are characterized by an optical spectrum with non-equidistant frequency spacing, as shown in Fig. 2(b) and (e), respectively. The difference between them lies in the irregular behavior spectrum, which also becomes broad and noisy, exhibiting low values of the comb line intensity-to-noise level ratio.

As in the case of CW injection, we say that PS to the orthogonal polarization of the VCSEL takes place when the power ratio between the two polarizations is greater than 20 dB in favor of the orthogonal one.

IL' refers to a state where the slave laser is frequency locked to the lines of the injected comb emitting in the orthogonal polarization (see Fig. 2(c)). However, due to the power modulation caused by the frequency comb injection, the optical spectrum of the IL' state is characterized by the presence of three optical lines [37] in contrast to the single optical line observed in CW operation. The appearance

of the additional comb lines is attributed to the nonlinear dynamics occurring within the injected laser. Specifically, the injected frequency comb induces a modulation of the carrier density at the modulation frequency.

Finally, we define the modulated-EPIL state when the VCSEL presents combs in both polarizations that are locked to the injected comb. This implies that both polarizations are excited at the injected frequency, as shown in Fig. 2(f).

## 3. Experimental setup

Fig. 3(a) shows the experimental all-fiber setup developed to inject light from a DML (Eblana Photonics EP1550-0-DM-H19-FM), the master laser, into a quantum-well single-mode 1550 nm VCSEL (Raycan, Co. RC330161-FFP pigtail VCSEL) with an InAlGaAs active region, the slave laser. The light is injected using a three-port optical circulator (OC). The VCSEL's output is analyzed by connecting different measurement equipment to the third port of the circulator. Our aim is to study the nonlinear dynamics found in the VCSEL when the DML is operated in two different regimes: (1) CW operation and (2) GS to generate a 3-line OFC.

In blue color we show the typical scheme to provide CW OI into the VCSEL [27–31]. At the output of the DML, an optical isolator is included to avoid optical feedback in the DML cavity. The first polarization controller (PC1) is used to control the polarization state of the light emitted from the DML and to achieve orthogonal optical injection. A variable optical attenuator (VOA) is included to control the level of the optical power of the externally injected signal. The second port of the circulator is connected to a 90/10 fiber coupler. The 90% branch is connected to the VCSEL, whereas the 10% branch is connected to a power-meter (PM1) to monitor the injected power into the VCSEL,  $P_{inj}$ . Finally, the output of the VCSEL is analyzed by connecting to the third port of the optical circulator a second PC (PC2) and a 50/50 coupler. The second PC2 is used to discriminate the two orthogonal polarizations of the VCSEL at the output of the polarization beam splitter (PBS) placed in the lower branch of the 50/50 coupler. The PBS has an extinction ratio of 20 dB. After the PBS, we measure using the power meters 2 and 3 the total amount of power present on each polarization. Orthogonal OI is attained by adjusting PC1 to maximize the power output from the DML at power meter 2 and adjusting PC2 to maximize the power output from the VCSEL at power meter 3. A third PC (PC3) is used to perform polarization resolved measurements of the optical spectra in a high-resolution (10 MHz) Brillouin Optical Spectrum Analyzer (BOSA 210 from Aragon Photonics), where both polarizations can be studied simultaneously. It is important to note that the polarization adjustment remains fixed for all measurements. When using the setup shown in Fig. 3(a), the optical spectra of the orthogonal polarization include the output of the VCSEL and the optical injection that is reflected at the VCSEL cavity. We have measured the amount of power reflected in the VCSEL cavity when it is turned off and the DML emits 600  $\mu$ W. The reflected power at the output of each branch of the 50/50 coupler is approximately 2.8%. The small magnitude of the reflected power ensures that its influence on our experimental results remains negligible.

The injection of an OFC is achieved by gain switching the DML, adding to the setup the parts in orange, i.e., the RF signal generator (Keysight N5173B) and the bias-tee shown in Fig. 3(a), enclosed by a dashed line. The bias-tee allows to drive the DML by the superposition of a DC bias current  $I_{bias,DML}$  and a sinusoidal modulation current provided by the RF signal generator. The OFC is also injected perpendicular to the linear polarization of the free-running VCSEL.

The optical spectrum of the total power of the free-running VCSEL at  $I_{bias,VCSEL} = 9.8$  mA and 28  $^{\circ}$ C is shown in Fig. 3(b). These bias current and temperature values are kept constant during all the experiments. The temperature and bias current of the VCSEL are controlled using a temperature controller (Thorlabs TED200C) and a current

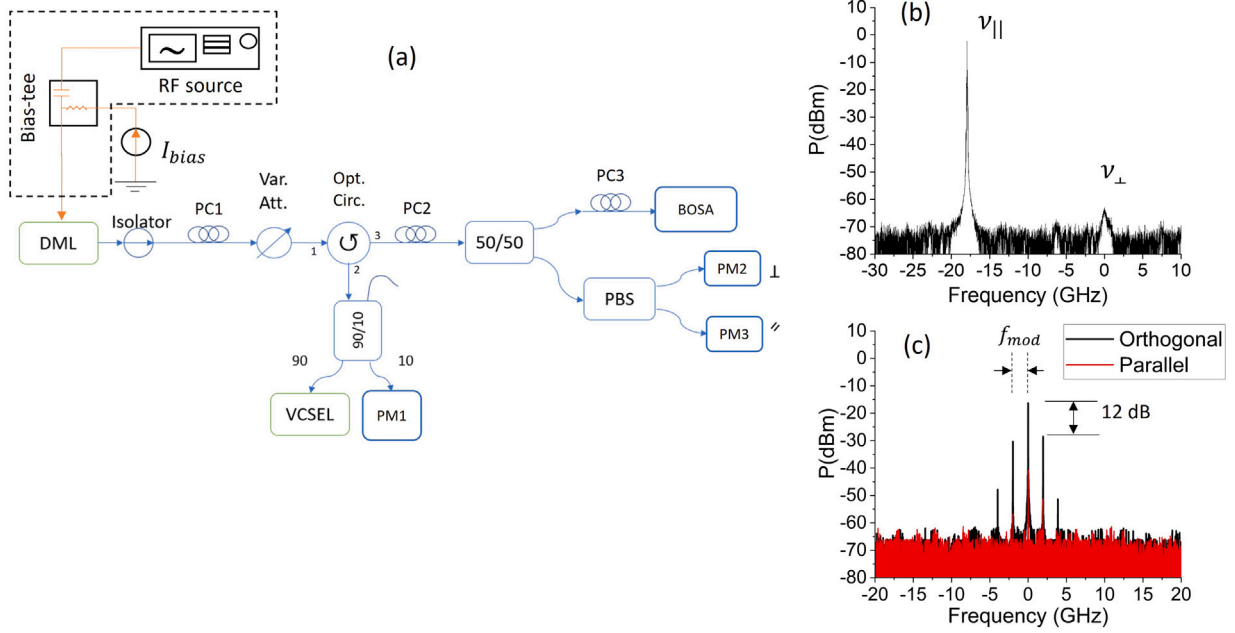


Fig. 3. (a) Representation of the experimental setup, (b) optical spectrum of the free-running VCSEL driven at  $I_{bias,VCSEL} = 9.8$  mA and  $T = 28$  °C and (c) optical spectrum of the injected OFC generated by the DML when  $I_{bias,DML} = 30$  mA,  $T = 25$  °C,  $f_{mod} = 2$  GHz and  $V_{RF} = 150$  mV.

controller (Thorlabs LDC200C), respectively. The VCSEL used in the experiment has a threshold current of  $I_{th,VCSEL} = 1.8$  mA at a temperature of 28 °C. PS from the short-wavelength to the long-wavelength polarization mode is observed at  $I_{PS} = 4.1$  mA.

In the optical spectrum shown in Fig. 3(b), we have chosen the zero frequency to correspond to the suppressed or “orthogonal” polarization of the VCSEL. This criterion will be used throughout the paper. We can observe that when  $I_{bias,VCSEL} = 9.8$  mA and at 28 °C, the orthogonal polarization is suppressed by 60 dB with respect to the dominant one. The VCSEL emits in the dominant or “parallel” polarization at wavelength  $\lambda_{\parallel} = 1547.06$  nm, which is shifted over 0.144 nm to the long wavelength side as compared to the “orthogonal” polarization. The frequency difference between the two orthogonal polarizations is 17.95 GHz, very similar to the birefringence of the VCSEL reported in [14]. However, note that in contrast to [14], at  $I_{bias,VCSEL} = 9.8$  mA the parallel polarization of our VCSEL appears on the shorter-frequency side of the optical spectrum (frequency  $\nu_{\parallel} < \nu_{\perp}$ ).

The threshold current of the DML used in the experiment is  $I_{th,DML} = 14$  mA and its modulation bandwidth is 10 GHz. The DML bias current,  $I_{bias,DML}$ , is controlled with a laser driver (Luzwavelabs LDC/E-Current200) and its temperature with a temperature controller (Luzwavelabs LDC/E-Temp3). In all the experiments the DML bias current is set at  $I_{bias,DML} = 30$  mA.

Fig. 3(c) shows the optical spectrum of the injected GS-OFC for  $f_{mod} = 2$  GHz and  $V_{RF} = 150$  mV. Under these conditions we prevent the pulses from being “switched off”, ensuring the coherence of the train of gain-switching pulses [19]. We aim at injection with orthogonal polarization, however, the parallel polarization observed in the optical spectrum of Fig. 3(c) is the result of an imperfect adjustment of the polarization in the BOSA due to the limitations of the setup. It can be seen from Fig. 3(c) that the injected comb spectrum comprises five equidistant lines, spaced at the modulation frequency, with only three of them having appreciable power. The side mode suppression ratio of the central and the nearest side lines is 12 dB, while the other lines are suppressed by more than 30 dB. Thus, we classify the injected comb as a 3-line OFC.

We define two different frequency detunings for the CW OI and the injection of an OFC, denoted as  $\Delta\nu_1$  and  $\Delta\nu_2$ , respectively. In the case of CW injection,  $\Delta\nu_1$  is defined as the frequency difference between

the externally injected signal,  $\nu_{inj}$ , and the orthogonal polarization of the free-running VCSEL,  $\nu_{\perp}$ , i.e.,  $\Delta\nu_1 = \nu_{inj} - \nu_{\perp}$ . On the other hand, when an OFC is injected,  $\Delta\nu_2$  is defined as the difference between the central frequency of the injected comb,  $\nu'_{inj}$ , and  $\nu_{\perp}$ , i.e.,  $\Delta\nu_2 = \nu'_{inj} - \nu_{\perp}$ . Throughout all the experiments,  $\Delta\nu_1$  and  $\Delta\nu_2$  are controlled by changing the temperature of the DML.

## 4. Experimental results and discussion

### 4.1. Nonlinear dynamics under orthogonal CW and GS-OFC injection

So far, theoretical [27] and experimental [27–29] reports on nonlinear dynamics maps of 1550 nm-VCSELs subjected to CW OI have focused on VCSELs with high birefringence values around 60 GHz [27–29], and with the parallel polarization appearing on the longer-frequency side of the optical spectrum ( $\nu_{\parallel} > \nu_{\perp}$ ). Moreover, these previous maps were obtained for the total power of the VCSEL without considering the dynamics of each polarization [27,28]. In [28], RF spectra of the total and polarized power have been reported, but just for specific frequency detunings. Solely in [29], polarization resolved nonlinear dynamics maps have been investigated. However, instead of spanning both polarizations of the VCSEL, these maps focus only on the dynamics found in the case of CW OI near the suppressed polarization of the free-running VCSEL. Different behaviors have been found, including IL, periodic dynamics, and chaos [27–29].

As compared to other 1550 nm-VCSELs reported in the literature, our VCSEL presents a smaller birefringence value (17.95 GHz) of the lasing mode or “parallel polarization” vs. “orthogonal polarization”, and the lasing mode is on the shorter-frequency side ( $\nu_{\parallel} < \nu_{\perp}$ ). To our knowledge, no studies have reported polarization-resolved nonlinear dynamics maps with this parameter configuration (17.95 GHz and  $\nu_{\parallel} < \nu_{\perp}$ ), involving OI spanning both polarizations of the free-running VCSEL, for either CW OI or injection of a GS-OFC.

In these maps (see Fig. 4(a)–(b)), we have represented the dynamics found in the orthogonal and parallel polarizations of the VCSEL using horizontal and vertical lines, respectively. Only the regions where irregular dynamics appear simultaneously in both polarizations are represented in gray color without a line pattern. The stars appearing in the maps indicate working points where we have experimentally

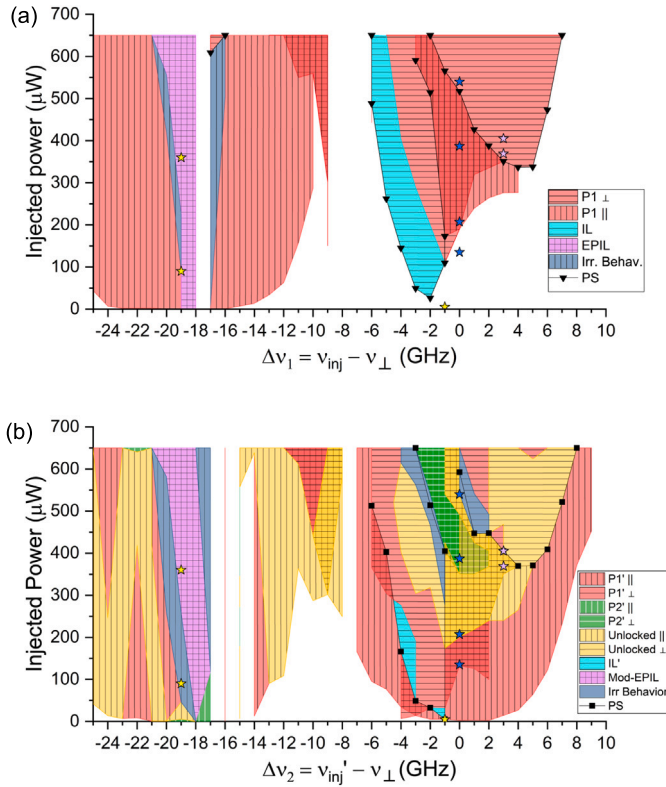


**Fig. 4.** Polarization resolved nonlinear dynamics maps of (a) CW injection and (b) GS-OFC injection when  $f_{mod} = 2$  GHz and  $V_{RF} = 150$  mV. The vertical and horizontal lines represent parallel and orthogonal polarizations, respectively. The observed dynamics are: P1 (period 1); P2, (period doubling); IL (injection locking), EPIL (elliptically polarized injection locking), Mod-EPIL (modulated EPIL); Unlocked dynamics; PS (polarization switching). The apostrophe notation indicates that the corresponding dynamics has been obtained under modulated injection. The stars mark the situations analyzed in Figs. 5, 6 and 7.

measured optical spectra of “representative” nonlinear dynamics. These will be analyzed in the following section in Figs. 5–7.

Hereafter, we refer to CW orthogonal optical injection simply as CW OI. Fig. 4(a) shows the polarization-resolved nonlinear dynamics map, in the plane of injected power vs. frequency detuning, when the VCSEL is subject to CW OI. The map has been experimentally obtained by fixing a value of  $\Delta v_1$ , in steps of 1 GHz, and increasing  $P_{inj}$  starting from low values. As we observed noteworthy changes in the optical spectrum’s dynamics, we recorded both the current injected power and the resulting nonlinear dynamic behavior. These data were then synthesized, linking points of analogous behaviors to delineate the different regions of the map. When we consider values of  $\nu_{inj}$  that are close to the orthogonal polarization of the free-running VCSEL, i.e., around  $\Delta v_1 = 0$  GHz, we observe regions of polarization switching (PS), injection locking (IL), or periodic behavior (P1) in one or both polarizations (see an illustrative example in Fig. 1(b)). These behaviors are consistent with those previously reported in VCSELs with a birefringence of 60 GHz and  $\nu_{||} > \nu_{\perp}$  [28,30,31].

The contours between the black triangles shown in Fig. 4(a) indicate the optical powers required to obtain PS. The PS trend is similar to those reported in [28,30,31], exhibiting a local minimum for positive values of  $\Delta v_1$ , and an absolute minimum when the frequency detuning is negative [31]. PS and IL occur simultaneously when  $-6$  GHz  $< \Delta v_1 < -1$  GHz, in agreement with [28,30,31]. In this region, we can observe that the injected power required for PS, increases as  $\Delta v_1$  decreases. The latter has also been found for VCSELs with the parallel polarization on the higher frequency side ( $\nu_{||} > \nu_{\perp}$ ) and with birefringence values of either 60 GHz [28,30,31] or 17.71 GHz [14].

Previous studies have reported that once the IL is achieved at negative frequency detunings, it is maintained over the entire range of injected power [28]. In contrast, Fig. 4(a) shows that P1 dynamics in the orthogonal polarization, can appear only if the injected power is sufficiently large.

Moreover, Fig. 4(a) shows that when  $\Delta v_1 \geq -1$  GHz, and the injected power is increased from low values, P1 dynamics can be observed before and after the PS. Within the range  $0$  GHz  $\leq \Delta v_1 \leq 4$  GHz, a small region with P1 dynamics in the parallel polarization can be observed. Our analysis of the optical spectra obtained from the BOSA for the specified region (not shown), indicates that as the injected power is increased, the amplitude of the only side peak that appears in the parallel polarization remains constant at 10 dB above the noise level. Although our analysis uncovers a single additional peak in the spectrum of the parallel polarization, and thus, according to our criteria, a P1 dynamic is considered, it is important to highlight that this peak’s marginal dominance over the noise level minimally contributes to the overall periodic dynamics of the system, which is consistent with findings from [28]. It is also worth pointing out the region  $-3$  GHz  $\leq \Delta v_1 \leq 3$  GHz, where P1 dynamics is found for both polarizations with significant power, contributing to the dynamics of the system. Our results are in good agreement with those presented in [28], where for  $\Delta v_1 > 4$  GHz and after PS, P1 dynamics were only observed in the orthogonal polarization, while for  $-2$  GHz  $\leq \Delta v_1 \leq 0$  GHz, P1 dynamics in both polarizations were found.

In addition, Fig. 4(a) also illustrates that in the region  $-9$  GHz  $< \Delta v_1 < -6$  GHz no dynamics were found. This contrasts with the results reported in the literature for VCSELs of 60 GHz and 17.71 GHz birefringence, where in this range of frequency detunings and injected powers, PS [14,28,31], periodic dynamics or IL were observed [27–29]. While birefringence does not appear to play a significant role, the observed differences could be related to the different relative position of the dominant and suppressed polarizations in the optical spectrum of the VCSEL, since in our case  $\nu_{||} < \nu_{\perp}$  while in those reported in the literature  $\nu_{||} > \nu_{\perp}$ . Due to the non-zero value of the linewidth enhancement factor of the VCSELs, frequency asymmetric behaviors have already been reported [28].

When we consider values of  $\nu_{inj}$  close to  $\nu_{||}$ , i.e., around  $\Delta v_1 = -17.95$  GHz, Fig. 4(a) presents regions of EPIL and irregular behavior. EPIL can be found when  $-21$  GHz  $< \Delta v_1 < -18$  GHz, in agreement with [39]. In this state, the VCSEL emits power in both polarizations (see Fig. 1(d)) at the injected frequency [39]. Irregular behavior arises in the boundaries of the EPIL region and is characterized by broad and irregular optical spectra in the parallel polarization (a schematic example of irregular behavior in both polarizations is shown in Fig. 1(c)). We see that above these irregular behavior regions, PS followed by P1 dynamics in the orthogonal polarization or EPIL can appear. The space between  $-17$  GHz and  $-18$  GHz has been intentionally left blank because with the resolution of the measurements (1 GHz), it is not possible to infer whether EPIL or irregular behavior is produced between both detuning values. A frequency detuning step of less than 1 GHz would be necessary to determine where the irregular behavior ends and where the EPIL begins. In addition, Fig. 4(a) also shows that P1 dynamics in the parallel polarization can be observed around  $\nu_{||}$ , i.e., around  $\Delta v_1 = -17.95$  GHz. A very small and narrow region, with P1 dynamics in both polarizations, also appears when  $-12$  GHz  $< \Delta v_1 < -9$  GHz.

In Fig. 4(b) we present the first polarization-resolved nonlinear dynamics map of the VCSEL when it is subject to the injection of a 3-line GS-OFC. The OFC which is driven at  $I_{bias,DML} = 30$  mA and features a modulation frequency of  $f_{mod} = 2$  GHz, and a modulation amplitude of  $V_{RF} = 150$  mV, as shown in Fig. 3(c), is injected orthogonally to the free-running polarization of the VCSEL. From now on, we refer to orthogonal GS-OFC injection simply as comb OI or modulated OI. The nonlinear dynamics map was experimentally obtained by fixing  $\Delta v_2$ , in steps of 1 GHz, and increasing the injected power  $P_{inj}$  starting from

low values following the same procedure as for Fig. 4(a). Compared to Fig. 4(a), (b) shows more complex dynamics including PS, IL', periodic combs (P1', P2'), unlocked dynamics, modulated-EPIL, and irregular behavior (see Fig. 2).

The contours with black squares in Fig. 4(b) show the optical powers required to obtain PS. Fig. 4(b) shows that the PS follows a similar trend as the PS obtained under CW OI. At negative frequency detunings, the injected power required for PS increases as  $\Delta v_2$  decreases. Moreover, a local minimum can be observed for positive values of  $\Delta v_2$ , while an absolute minimum occurs at  $\Delta v_2 = -1$  GHz. By comparing Fig. 4(a) and (b), it can be seen that the injected power needed to achieve PS is typically greater for modulated than for CW OI, except when  $\Delta v_2 = -1$  GHz,  $\Delta v_2 = -3$  GHz and  $\Delta v_2 \geq 6$  GHz. The PS curves resulting from CW and modulated OI were also analyzed in Ref. [14]. Our results differ from those reported in [14], particularly regarding the power necessary to achieve PS. Indeed, in [14], it was reported that PS required greater power in case of comb OI as compared to CW OI, but only for positive frequency detunings relative to the suppressed polarization of the free-running VCSEL.

We can also observe in Fig. 4(b) that PS and IL' occur simultaneously when  $-5 \text{ GHz} < \Delta v_2 \leq -1 \text{ GHz}$ . Once IL' is achieved, further increase of the injected power leads to the emergence of P1' combs, unlocked dynamics, or irregular behavior in the orthogonal polarization of the VCSEL. For frequency detunings within the range  $0 \text{ GHz} < \Delta v_2 < 8 \text{ GHz}$  and at injected powers exceeding those needed for PS, P1' combs, irregular behavior, and unlocked dynamics in the orthogonal polarization of the VCSEL are also observed.

When  $-3 \text{ GHz} < \Delta v_2 < 4 \text{ GHz}$ , we see unlocked dynamics and P1' combs appear, as well as P2' combs in both polarizations of the VCSEL simultaneously. Schematic examples of these are shown in Fig. 2(a) and (d), illustrating P1' and P2' combs, respectively. Similar OFCs were reported in [14] for frequency detunings between both polarizations of the free-running VCSEL.

Small regions where both polarizations of the VCSEL are excited, exhibiting unlocked dynamics or P1' combs also appear when  $\Delta v_2 < -3 \text{ GHz}$ . For frequency detunings in the range of  $-25 \text{ GHz} < \Delta v_2 < -9 \text{ GHz}$ , PN' combs as well as unlocked dynamics in the parallel polarization of the VCSEL can be observed. Nevertheless, it is worth noting that when analyzing the optical spectra from the BOSA (not shown), only a few additional lines typically emerge in these OFCs, and their amplitude, relative to the noise level, is usually very low, with minimal or no contribution to the system dynamics. As a result, these regions can be classified as regions of no 'interesting' dynamics for OFC generation. These results contrast with the findings of [14] where PN' combs, in one or both polarizations of the VCSEL, with a significant power and number of lines, were also observed in the region  $-18 \text{ GHz} < \Delta v_2 < 0 \text{ GHz}$ . The discrepancies between our findings and prior results [14] may be attributed to the different relative position of the dominant and suppressed polarizations in the optical spectrum of the free running VCSEL.

Additionally, when we consider values of  $v'_{inj}$  close to  $v_{\parallel}$  (i.e.,  $\Delta v_2$  around  $-17.95 \text{ GHz}$ ), two small regions with irregular behavior (as schematically shown in Fig. 2(e)), as well as a region of modulated-EPIL (see Fig. 2(f)), can be observed. To our knowledge this is the first time that modulated-EPIL has been observed under comb OI. As in Fig. 4(a), the space between  $-17 \text{ GHz} < \Delta v_2 < -15 \text{ GHz}$  has been intentionally left blank because with the resolution of the measurements (frequency detuning steps of 1 GHz) it was not possible to infer the corresponding dynamical state. Fig. 4(b) demonstrates that different types of optical frequency combs can be obtained at the output of the VCSEL by tuning the injection parameters.

#### 4.2. Comparing optical spectra from nonlinear dynamics under CW and GS-OFC injection

Fig. 5 shows the polarization-resolved optical spectra obtained at the VCSEL output for the most representative dynamical regimes. The

figure is divided into two rows: the top row shows the optical spectra obtained under CW OI at a fixed frequency detuning of  $\Delta v_1 = 0 \text{ GHz}$ , while the bottom row presents the optical spectra obtained under modulated OI at a fixed frequency detuning of  $\Delta v_2 = 0 \text{ GHz}$ . The output spectra for increasing values of injected power are shown in both rows. The working points yielding the optical spectra presented in Fig. 5 are marked with blue stars in Figs. 4(a) and (b) for CW and modulated OI, respectively.

When  $P_{inj} = 135 \text{ } \mu\text{W}$  under CW OI, Fig. 5(a) shows the optical spectrum obtained before reaching the P1 region where both polarizations of the VCSEL are excited. Two peaks in the optical spectrum can be observed. The peak that appears at  $-20 \text{ GHz}$  corresponds to the parallel polarization of the VCSEL while the peak that appears at  $0 \text{ GHz}$  corresponds to the injected light. In this case, no dynamics is observed.

Fig. 5(b) shows, for the same injected power, the optical spectrum obtained when the 3-line OFC shown in Fig. 3(c) is injected into the VCSEL. The optical spectrum is composed of two OFCs, one in each polarization, with the same frequency spacing. The frequency difference between the comb lines corresponds to the modulation frequency of the injected comb, i.e.,  $f_{mod} = 2 \text{ GHz}$ . We denote this dynamical regime as a P1' comb in both the parallel and orthogonal polarizations, in agreement with Fig. 4(b), because the frequency separation between consecutive lines of the optical spectrum for each polarization is given by  $f_{mod}/N'$  with  $N' = 1$ . It is worth mentioning that the presence of comb lines at the frequency of orthogonal (parallel) polarization in the optical spectra of the parallel (orthogonal) polarization are due to the extinction ratio of the experimental setup.

Increasing the injected power to  $P_{inj} = 207 \text{ } \mu\text{W}$  under CW OI, Fig. 5(c) shows the appearance of two strong sidebands at approximately 5 GHz on each side of the main peaks, which correspond to the parallel and orthogonal polarized power. This leads to the emergence of an incipient P1 dynamics in both polarizations. This is because the CW OI enhances the relaxation oscillations at the relaxation oscillation frequency (ROF) of the VCSEL ( $\nu_{ROF} \approx 5 \text{ GHz}$ ). When an OFC is injected into the VCSEL for the same injected power, unlocked dynamics appear in each polarization. As shown in Fig. 5(d) the modulated OI results in the emergence of sidebands around  $\nu_{\parallel}$  and  $\nu_{\perp}$  at a frequency separation equal to the modulation frequency ( $f_{mod} = 2 \text{ GHz}$ ). These spectral lines are embedded between  $\nu_{\parallel}$ ,  $\nu_{\perp}$  and the corresponding ROF spectral lines. The resulting spectra of each polarization exhibit an irregular line spacing, leading to the nonlinear dynamic that we refer as unlocked dynamics.

Fig. 5(e) depicts the effect of further increasing  $P_{inj}$  to  $387 \text{ } \mu\text{W}$  under CW OI. A clear P1 dynamics can be observed in both polarizations. Compared to Fig. 5(c), an increase in the injected power results in undamped relaxation oscillations dynamics, the sidebands become stronger, and extra peaks appear in the spectra of both polarizations at higher harmonics. This is due to the not sinusoidal nature of the oscillations. For the same injected power under modulated OI, Fig. 5(f) shows an optical spectrum characteristic of a P2' comb in both the parallel and the orthogonal polarization. The frequency spacing of the corresponding combs is  $\Delta f' = 1 \text{ GHz}$ . According to our definition of a PN' comb, this regime corresponds to a P2' comb as  $f_{mod} = 2 \text{ GHz}$ ,  $\Delta f' = 1 \text{ GHz}$ , and then  $N' = 2$ . Compared to Fig. 5(d), in Fig. 5(f) the injection power is high enough to enable the injected comb to lock with the P1 dynamics obtained under CW OI shown in Fig. 5(e), generating frequency beatings at 1 GHz. Fig. 5(f) illustrates that the bandwidth of the comb generated at the VCSEL's output is significantly broader than the bandwidth of the injected comb (see Fig. 3(c)). Specifically, the bandwidth is 43.6 GHz in Fig. 5(f) compared to 8 GHz in Fig. 3(c). The bandwidth is calculated as the frequency span (in GHz) covered by all the spectral lines exceeding 10 dB above the noise level.

When  $P_{inj} = 540 \text{ } \mu\text{W}$ , the injected power is high enough to achieve PS under CW OI in Fig. 5(g), but not under modulated OI in Fig. 5(h), consistent with the maps presented in Fig. 4. Fig. 5(g) displays the P1 dynamics obtained in the orthogonal polarization once the PS has

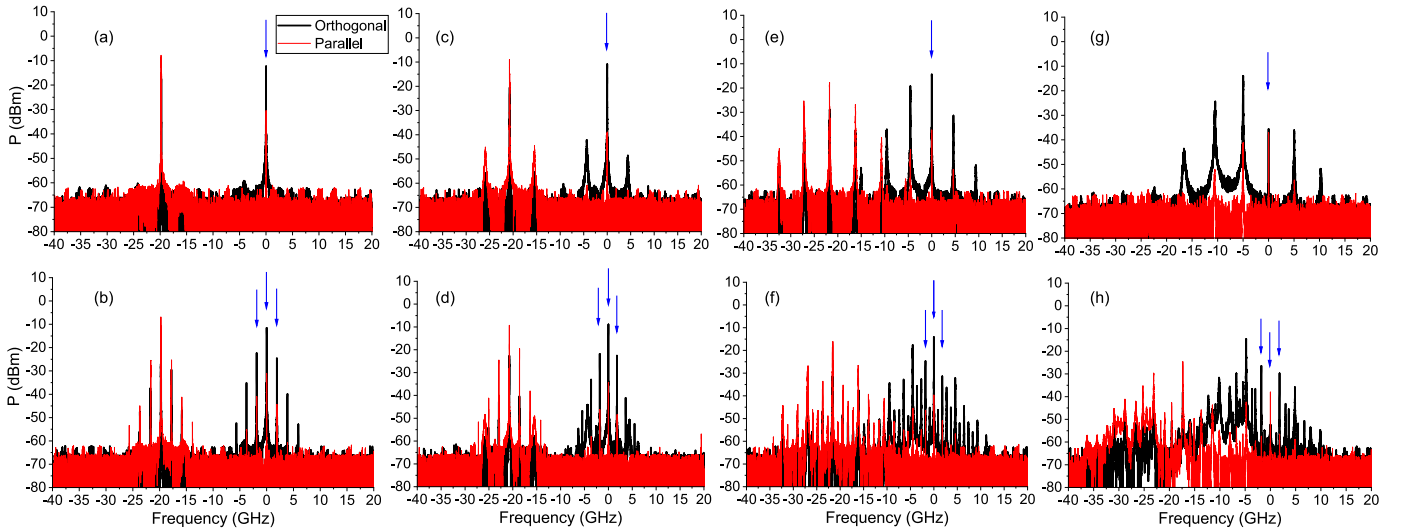


Fig. 5. Optical spectra of the polarized power at  $\Delta v_{1,2} = 0$  GHz. Panels (a), (c), (e), and (g) depict the results for CW OI at 135  $\mu\text{W}$ , 207  $\mu\text{W}$ , 387  $\mu\text{W}$ , and 540  $\mu\text{W}$ , respectively. Correspondingly, panels (b), (d), (f), and (h) illustrate the results for comb OI at the same power levels.

occurred, while in Fig. 5(h) the increase of the injected power leads to an irregular behavior characterized by a noisy and broad spectrum in both polarizations.

As discussed in Fig. 4, the injected power needed to achieve PS is typically greater for modulated than for CW OI. This situation is illustrated in Fig. 6 for  $\Delta v_{1,2} = 3$  GHz and two different values of injected power:  $P_{inj} = 369$   $\mu\text{W}$  in Fig. 6(a) and (b) and  $P_{inj} = 405$   $\mu\text{W}$  in Fig. 6(c) and (d). The working points yielding the optical spectra depicted in Fig. 6 are represented by purple stars in Fig. 4(a) and (b) for CW and modulated OI, respectively. When  $P_{inj} = 369$   $\mu\text{W}$ , Fig. 6(a) shows that PS has occurred under CW OI and P1 dynamics only in the orthogonal polarization can be observed. However, Fig. 6(b) shows that PS has not yet happened under modulated OI. Instead, an unlocked dynamics with wave-mixing frequency components in both polarizations can be observed. For a slightly higher injected power, i.e.,  $P_{inj} = 405$   $\mu\text{W}$ , Fig. 6(c) and (d) show that PS is found under both types of OI. Fig. 6(d) shows a P1' comb in the orthogonal polarization while the parallel polarization is suppressed. In this case, the frequency separation between the comb lines corresponds to the modulation frequency of the injected comb, i.e.,  $f_{mod} = 2$  GHz. Fig. 6(d) provides another example, illustrating that the bandwidth of the orthogonal comb generated at the VCSEL's output is broader than the bandwidth of the injected comb (see Fig. 3(c)). Specifically, the bandwidth in Fig. 6(c) is 26.8 GHz, while that of the injected comb (Fig. 3(c)) is 8 GHz.

In Fig. 7 we present the optical spectra corresponding to the dynamical behaviors indicated by the yellow stars in Fig. 4(a) and (b) for CW and modulated OI, respectively. In Fig. 7(a) and (b), OI is performed at  $\Delta v_{1,2} = -1$  GHz and  $P_{inj} = 5$   $\mu\text{W}$ . Fig. 7(a) shows two peaks corresponding to the injected frequency at  $-1$  GHz and the parallel polarization of the VCSEL at around  $-19$  GHz, respectively. Similar to Fig. 5(a), no dynamics is observed. Nevertheless, in Fig. 7(b), under modulated OI and when  $P_{inj} = 5$   $\mu\text{W}$ , simultaneous PS and IL' are achieved, as shown in Fig. 4(b). The VCSEL is frequency locked to the injected comb, emitting in the orthogonal polarization while the parallel polarization is suppressed. The resulting VCSEL output is not steady; instead, it is modulated at  $f_{mod} = 2$  GHz. A similar injection locked state was also observed in [14,37]. Fig. 7(c) and (d) show the optical spectra obtained when  $\Delta v_{1,2} = -19$  GHz and  $P_{inj} = 90$   $\mu\text{W}$ . Irregular behavior in the parallel polarization can be observed under both types of OI. The optical spectra exhibit an extensive and noisy pedestal with uneven frequency intervals and a relatively low ratio of comb line intensity to noise level for most frequencies.

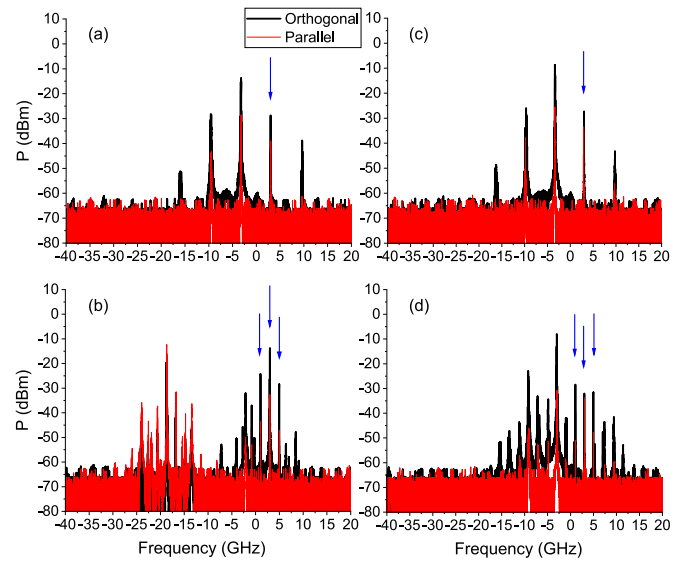


Fig. 6. Optical spectra of the polarized power at  $\Delta v_{1,2} = +3$  GHz. Panels (a) and (c) illustrate the results for CW injection at 369  $\mu\text{W}$  and 405  $\mu\text{W}$ , respectively. In parallel, panels (b) and (d) display the results for comb OI at the same power levels.

At the same frequency detuning, when increasing the injected power to  $P_{inj} = 360$   $\mu\text{W}$ , EPIL dynamics is observed under CW OI (Fig. 7(e)) while modulated-EPIL occurs under comb OI (Fig. 7(f)). In Fig. 7(e) the two polarizations of the VCSEL are excited and frequency locked to the master laser. This serves as a strong indication of the EPIL state [32,39]. Similarly, in Fig. 7(b), the two polarizations of the VCSEL are also excited and frequency locked to the master laser; however, due to the modulated OI, the VCSEL output is not steady as in Fig. 7(e). Instead, it is modulated at  $f_{mod} = 2$  GHz. This is the first time that this behavior, which we call modulated-EPIL, has been observed under modulated OI.

As already pointed out in the previous section, Fig. 4(b) demonstrates that under modulated OI, different types of optical frequency combs can be obtained at the VCSEL output by tuning the injection parameters. We have shown in Figs. 5, 6, and 7 the optical spectra corresponding to the different representative dynamic behaviors observed under comb OI. Similar behaviors have been reported for specific injection parameters in [14,38], but modulated-EPIL is reported here for the first time. In addition, in the next section we clarify the physical

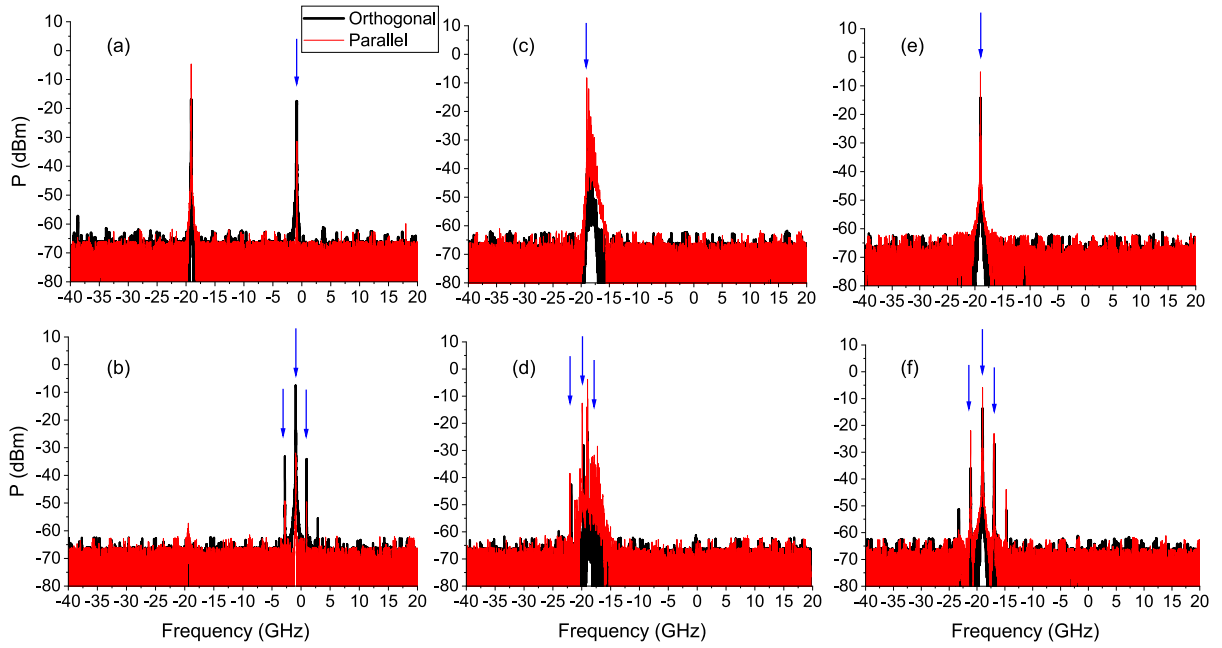


Fig. 7. Optical spectra of the polarized power. Panels (a), (c), and (e) illustrate the results for CW injection. Panels (b), (d), and (f) display the results for comb OI. In (a–b),  $\Delta v_{1,2} = -1$  GHz and  $P_{inj} = 5$   $\mu$ W; in (c–d)  $\Delta v_{1,2} = -19$  GHz and  $P_{inj} = 90$   $\mu$ W; and in (e–f)  $\Delta v_{1,2} = -19$  GHz and  $P_{inj} = 360$   $\mu$ W.

mechanism that drives the generation of combs with specific properties at the VCSEL output. Since the regions near  $v_{||}$  do not have interesting dynamics for OFC generation, in the following section we will focus our analysis only on the regions near  $v_{\perp}$ , i.e., for frequency detunings ranging from  $-7$  GHz to  $9$  GHz. We will also study the contour overlays of the nonlinear dynamics maps for CW OI and comb OI. These are also the regions relevant for the expansion of the injected comb, as we will demonstrate later on.

#### 4.3. Nonlinear dynamics contour overlays for CW and frequency comb injections

Fig. 8 illustrates the contours of the regions of the CW OI map from Fig. 4(a) in black with solid thin lines, overlaid with the contours of the regions of the comb OI map from Fig. 4(b) in blue with dashed lines. Both maps are depicted only in the vicinity of  $v_{\perp}$ , i.e.  $-7$  GHz  $\leq \Delta v_{1,2} \leq 9$  GHz. The stars in the map represent the working points yielding the optical spectra from Figs. 5 and 6 used to illustrate the nonlinear dynamics obtained under both types of OI. Our results show that the VCSEL's nonlinear dynamics induced by the OI of a 3-line GS-OFC, are mainly influenced by two factors: (1) the frequencies of the VCSEL's nonlinear dynamics under continuous-wave OI, and (2) the PS curves obtained under both types of OI. The PS curve under CW OI (modulated OI) is represented by the contour between the black triangles (blue squares). The regions of interest for OFC generation are highlighted in green in Fig. 8. In these regions the dynamics obtained under CW OI determine the type of combs obtained at the VCSEL's output under modulated OI.

Examining the areas labeled 1 and 2 in Fig. 8, in conjunction with Fig. 4(a) and (b), we observe that in these regions 1 and 2, dynamics is exclusively present in the orthogonal polarization of the VCSEL for both CW and modulated OI. For those values of  $P_{inj}$  and frequency detunings, PS has already occurred in both OI scenarios. For CW OI, the orthogonal polarization of the VCSEL exhibits P1 dynamics (see Fig. 4(a)). In contrast, upon injecting a comb, the P1 dynamics in the orthogonal polarization change to different types of dynamics, including P1' combs, unlocked dynamics, or irregular behavior (see Fig. 4(b)). In the region labeled 3 in Fig. 8, both polarizations are excited under both types of OI, as can be observed in Fig. 4(a) and (b).

Under CW OI, the VCSEL exhibits P1 dynamics in both polarizations. However, when a comb is injected, the P1 dynamics of these polarizations are transformed into P2' combs or unlocked dynamics. The underlying physical mechanism responsible for the dynamics observed at the VCSEL output when injecting the comb is the beating between the frequencies of the CW P1 dynamics and those of the injected comb.

Periodic combs are produced when the beating generates frequencies that are harmonically related to the P1 oscillation frequency under CW OI. This phenomenon is illustrated by the optical spectra in Fig. 5(e) and (f) for  $P_{inj} = 387$   $\mu$ W and  $\Delta v_2 = 0$  GHz, corresponding to a star in region 3 in Fig. 8. The periodic comb produced at the VCSEL output exhibits a frequency spacing of  $\Delta f' \approx 1$  GHz (see Fig. 5(f)). This frequency spacing results from the beating between the spectral components of the injected comb, separated by the modulation frequency ( $f_{mod} = 2$  GHz), and the spectral components corresponding to the P1 dynamics obtained under CW OI, separated by  $\approx 5$  GHz (see Fig. 5(e)). The frequency spacing of the resulting comb,  $\Delta f' \approx 1$  GHz, corresponds to half of the modulation frequency, giving rise to a P2' comb in both polarizations. An additional example can be observed for  $P_{inj} = 405$   $\mu$ W and  $\Delta v_{1,2} = 3$  GHz by comparing Fig. 6(c) and (d). These spectra correspond to a star in region 2 of Fig. 8, where only the orthogonal polarization presents dynamics under both types of OI. In this case, the beating between the spectral components of the CW P1 dynamics separated by  $6$  GHz and the spectral components of the injected comb separated by  $f_{mod} = 2$  GHz, generates a P1' comb at the VCSEL output. As evidenced in Fig. 6(d), the ensuing comb displays a frequency spacing of  $\Delta f' = 2$  GHz.

As mentioned above, for our specific injected comb, in regions 1 and 2 comb generation under modulated OI is possible exclusively in the orthogonal polarization, as only this polarization displays dynamics under CW OI. However, in region 3, comb formation under modulated OI is feasible with both polarizations excited, as both polarizations of the VCSEL exhibit dynamics under CW OI. Moreover, for each polarization we consider the width of its corresponding optical spectrum as the total span of the frequency range covered by all the individual lines. In regions 1–3, the comb widths acquired for each polarization under modulated OI, coincide with the widths of the spectra of the P1 dynamics observed for each polarization under CW OI, as shown in Fig. 5(e) and (f) and Fig. 6(c) and (d).

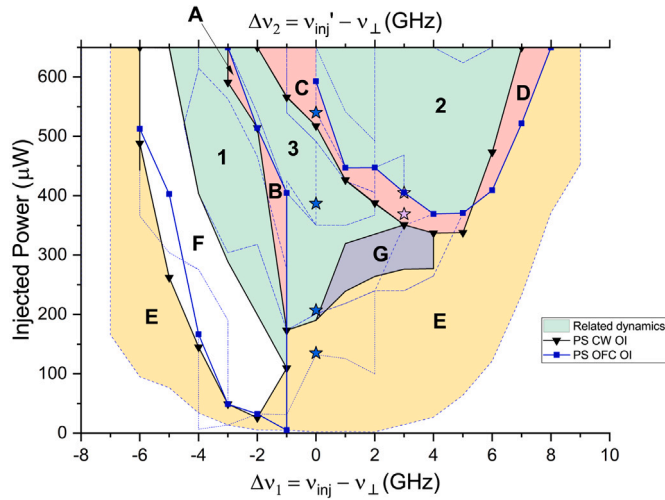


**Fig. 8.** Overlay map of CW and comb injection nonlinear dynamics in the vicinity of  $v_{\perp}$ . Nonlinear dynamics regions' contours under CW and comb injection are illustrated in black with solid thin lines and in blue with dashed lines, respectively. The PS curves under CW and comb OI are represented by the contour between the black triangles and the blue squares, respectively. Regions 1–3 represent areas where there is a shared relationship between the CW nonlinear dynamics and those produced by comb OI, whereas regions A–G denote the areas where both dynamics are not related.

In addition, in regions 1–3, unlocked dynamics can also be found under comb OI for certain values of  $P_{inj}$  and frequency detunings. These non-locking regions are identified as regions where the spectra have an irregular frequency spacing without a noise pedestal (see schematic in Fig. 2(b)). The unlocked dynamics can be generated through nonlinear mixing processes between the CW P1 dynamics and the injected comb, or as a result of sidebands generated by the injected comb around each line of the optical spectrum corresponding to the CW P1 dynamics. The spacing between these sidebands is determined by the modulation frequency of the injected comb, which is typically not a multiple or submultiple of the P1 oscillation frequency obtained in CW OI. Consequently, the resulting comb at the VCSEL output exhibits an irregular frequency spacing. An example of unlocked dynamics is shown in Fig. 5(d) for  $\Delta v_2 = 0$  GHz and  $P_{inj} = 207$   $\mu$ W. This optical spectrum lies within the region 3 and is marked with a star in Fig. 8. The modulated injection induces sidebands around  $v_{\parallel}$  and  $v_{\perp}$  separated by the modulation frequency ( $f_{mod} = 2$  GHz). These sidebands are located between the frequencies corresponding to the relaxation oscillation frequencies. It can also be seen that owing to a wave mixing process between the P1 dynamics derived from CW OI (Fig. 5(c)) and the frequency components produced under modulated OI, additional frequencies emerge in the optical spectrum corresponding to the orthogonal polarization. As a result, the ensuing comb at the output of the VCSEL exhibits irregular spacing.

Irregular behavior arises from a wave mixing process involving the CW P1 dynamics and the injected comb, which occurs when no frequencies harmonically related to the P1 oscillation frequency under CW OI are generated. Such behaviors are characterized by not only an irregular frequency spacing but also a wide noise pedestal in the spectrum (see schematic in Fig. 2(e)). As can be seen in Fig. 4(b), the irregular behavior tends to be observed in the areas close to the PS.

We thus find that regions 1–3 represent areas where there is a shared relationship between the nonlinear dynamics provoked by CW OI and those produced by comb OI. This allows us to understand the physical origin of the width, the polarization and the characteristics of the comb obtained at the VCSEL output.

In regions A–D in Fig. 8, the dynamics obtained under modulated and CW OI are not related due to the mismatch in injection powers required to achieve PS. Consequently, it is possible to observe scenarios

where both polarizations are excited in CW OI while only one is excited under modulated OI, or vice-versa (see Figs. 5(g–h) and 6(a–b) which are marked with stars in region C of Fig. 8).

Under CW OI, region E is characterized by the absence of dynamics, region F exhibits IL and region G displays P1 dynamics in the parallel polarization. These dynamics bear no relation to those observed at the VCSEL output under modulated OI. This can be observed by comparing the dynamics shown in the maps of Fig. 4(a) and (b) in regions E, F and G. In region E, under comb OI, P1' combs can appear in the parallel polarization or in both polarizations, while no dynamics are observed under CW OI. In region F, IL' or P1' combs in the orthogonal polarization can be found, while only IL is observed under CW OI. In region G, in the presence of comb OI, unlocked dynamics in the parallel polarization or in both polarizations can be found while P1 dynamics in the parallel polarization appears under CW OI. It is also important to note that the CW P1 dynamics obtained in region G is not particularly interesting for OFC generation. As previously mentioned, only a few additional lines emerge in the optical spectrum (not shown), and these have a very low amplitude relative to the noise level.

In conclusion, knowing the dynamics involved in CW OI offers valuable insights to understand the characteristics of the frequency combs produced at the VCSEL's output, specifically within regions 1–3. We find that when the beating between the injected comb and the CW P1 dynamics generates frequencies harmonically related to  $f_0$ , a periodic comb can be achieved.

In regions 1 and 2, combs with orthogonal polarizations can be generated. Conversely, in region 3, it is possible to generate combs in both polarizations of the VCSEL, making this region particularly attractive for acquiring wider frequency combs. This is illustrated in the next section. As previously mentioned, the width of the combs generated in regions 1–3 aligns with the width of the CW P1 dynamics. It is important to remark that these observations apply only to our specific comb injection conditions (i.e. 3 comb lines with  $f_{mod} = 2$  GHz and  $V_{RF} = 150$  mV) and cannot be generalized for a generic injected OFC with different modulation frequencies and or different modulation amplitudes.

#### 4.4. Mapping of the P1 oscillation frequency and optical spectra width under orthogonal CW injection

As previously discussed, knowing the dynamics of the CW OI within certain regions enables us to comprehend the width, polarization, and characteristics of the combs generated at the VCSEL's output. When the beating between the injected comb and the CW P1 dynamics generates frequencies harmonically related to  $f_0$ , a periodic comb can be achieved. Therefore, Fig. 9 presents the polarization-resolved mapping of the P1 oscillation frequency,  $f_0$ , along with the total width of the optical spectrum stemming from the P1 dynamics, generated via CW OI. The map is presented in the plane of injected power versus frequency detuning ( $\Delta v_1$ ) spanning both polarizations of the free-running VCSEL.

The figure displays lines representing constant P1 oscillation frequency  $f_0$ . These are illustrated by solid lines, red for parallel polarization and black for orthogonal polarization, respectively. Using the same color scheme, dashed lines demarcate the boundaries of the P1 regions for each polarization. The numerical values in red (black) depicted on these lines represent the  $f_0$  value in GHz for the parallel (orthogonal) polarization. The value of the P1 oscillation frequency, at the boundaries of the P1 region, falls within the values of the two adjacent solid lines intersecting the delineating dashed line.

The map was experimentally generated by setting a fixed value for  $\Delta v_1$  in 1 GHz increments, and progressively increasing  $P_{inj}$  starting from low values. For each  $P_{inj}$ , we measured the P1 oscillation frequency,  $f_0$ , and the total width of the optical spectrum. The measurement of  $f_0$  was accomplished by assessing the frequency separation within the spectral components of each polarization present in the optical spectrum of the CW P1 dynamics as illustrated in Fig. 1(b).

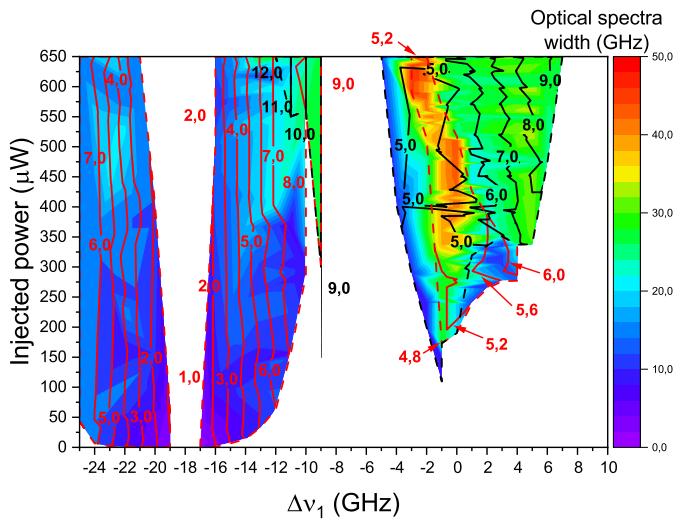


**Fig. 9.** Polarization resolved mapping of the P1 oscillation frequency,  $f_0$ , and optical spectral width obtained under CW OI. Red and black lines respectively denote unvarying P1 oscillation frequencies for parallel and orthogonal polarizations, respectively. The boundaries of P1 regions for each polarization are outlined using dashed lines, with red and black colors corresponding to parallel and orthogonal polarizations, respectively. Aligned with this color coding, numerical values indicate the  $f_0$  values in GHz for parallel and orthogonal polarizations. The complete width of the CW P1 dynamics spectrum is illustrated via a color map.

When  $-5 \text{ GHz} < \Delta\nu_1 < 7 \text{ GHz}$ , it can be observed that for low injected power, the numerical values of the lines indicate that  $f_0$  is close to the relaxation oscillation frequency ROF (approximately 5 GHz) for both polarizations. However, as the injected power increases, a frequency pushing effect [28] becomes evident, resulting in a shift of  $f_0$  towards higher frequency values. An increase of  $P_{inj}$  enhances the stimulated recombination of carriers, leading to a smaller carrier density. As a result, the refractive index and the wavelength of the orthogonal polarization increase giving rise to a larger frequency detuning and then an increased  $f_0$  value. Conversely, when  $-25 \text{ GHz} < \Delta\nu_1 < -9 \text{ GHz}$ ,  $f_0$  closely corresponds to  $|\Delta\nu_1 + 18| \text{ GHz}$ , rendering the  $f_0$  curves nearly parallel to a frequency detuning that matches the expected frequency detuning if measured with respect to the parallel polarization of the free-running VCSEL, i.e.,  $\Delta\nu = \nu'_{inj} - \nu_{\parallel}$ .

The total width of the spectrum of the CW P1 dynamics is illustrated in Fig. 9 by the color map. For each polarization, we estimate its optical spectral width as the frequency span (in GHz) covered by all the lines exceeding 10 dB above the noise level. When both polarizations have dynamics, the total width equals the sum of individual widths, unless their dynamics spectrally overlap. In the case of overlapping dynamics, the width of the spectrum is calculated from the first to the last of the qualifying spectral lines, regardless of their association with either polarization, thus not double-counting the overlap region's contribution to the optical spectral width. Three main areas can be distinguished when  $-5 \text{ GHz} < \Delta\nu_1 < 7 \text{ GHz}$ . First there is a blue sector with widths between 10 GHz and 20 GHz, aligning with optical spectra comprising approximately 2 to 4 spectral components, akin to those in Fig. 5(c). A green sector is also present, displaying widths between 24–32 GHz mainly in the orthogonal polarization, similar to the optical spectra shown in Fig. 6(a) and (c). A final orange sector is observed, where there is a noticeable increase in spectral widths, reaching approximately 50 GHz. This last sector is especially intriguing for achieving broader optical frequency combs due to the excitation of both polarizations of the VCSEL. In fact, we have found that the OFCs obtained under modulated OI in this sector can also match these substantial widths.

When  $-25 \text{ GHz} < \Delta\nu_1 < -9 \text{ GHz}$ , the map is predominantly blue indicating optical spectra in the parallel polarization with widths

approximately between 1 GHz and 20 GHz. These optical spectra contain merely 3 or 4 spectral components. A minor green sector where both polarizations are excited becomes evident when  $-12 \text{ GHz} < \Delta\nu_1 < -9 \text{ GHz}$ . However, as noted in the previous sections, the region spanning  $-25 \text{ GHz} < \Delta\nu_1 < -9 \text{ GHz}$ , despite its limited spectral components, also displays notably low power levels in these components. Consequently, these contribute minimally to the system's dynamics.

## 5. Discussion and conclusions

Dombia et al. identified that the OI of a 3-line optical frequency comb into a VCSEL could effectively modify the OFCs generated at the VCSEL's output [14]. In this paper, we have revealed the underlying physics through an exhaustive analysis of polarization-resolved nonlinear dynamics maps of a 1550 nm-VCSEL, subjected to two distinct types of orthogonal optical injection: continuous-wave injection and injection of a 3-line gain-switched OFC. These maps were realized in the plane of injected power versus frequency detuning and span both polarizations of the free-running VCSEL.

Our study presents the first polarization-resolved nonlinear dynamics maps of a VCSEL with a small birefringence below 20 GHz and  $\nu_{\parallel} < \nu_{\perp}$ , covering both types of optical injections. As far as we know, nonlinear dynamics maps for VCSELs with these specific parameters have not been reported in the literature.

By pushing beyond previous investigations [14,38], we have gained deeper insights into the nonlinear behaviors that VCSELs exhibit under the influence of OI from a 3-line GS-OFC. Firstly, under CW OI, we have identified boundaries between regions of different behavior, including P1 dynamics in one or both polarizations, IL, EPIL, irregular behavior, and PS. We have found that PS and IL can occur simultaneously. Notably, the optical power required for PS follows a similar trend to that reported in previous research, showing a local minimum for positive values of  $\Delta\nu_1$  and an absolute minimum when the frequency detuning is negative [31]. The injected power required for PS increases as the frequency detuning decreases. The latter has been found for VCSELs with  $\nu_{\parallel} > \nu_{\perp}$ , and with birefringence values of either 60 GHz [28,30,31] or 17.71 GHz [14].

Secondly, the application of GS-OFC injection further enriched the complexity of the observed dynamics, exhibiting behaviors such as PS, IL', P1', P2' combs, unlocked dynamics, and modulated-EPIL, among others. This has been the first time that modulated-EPIL has been observed. Moreover, we have also found a region where it is possible to obtain P1' and P2' combs with approximately 50 GHz width, similar to [14].

Our analysis demonstrates that the VCSEL's nonlinear dynamics induced by the OI of a 3-line GS-OFC, are largely influenced by two factors: the frequencies of the nonlinear dynamics under CW OI, and the polarization switching curves under both types of OI. Consequently, our work facilitates a more comprehensive understanding of the OFCs produced at the VCSEL's output, guided by the CW nonlinear dynamics map and the polarization switching curves that this study provides.

Particularly, we have identified several distinct regions, 1, 2 and 3, in Fig. 8 for GS-OFC injection, where the type of combs produced at the VCSEL's output show a clear alignment between the dynamics, polarization, and width of the spectra observed under CW OI. We have found that within regions 1 and 2, combs with orthogonal polarizations can be generated while in region 3, it is feasible to generate combs in both polarizations of the VCSEL, making this region particularly attractive for producing wider frequency combs. Moreover, we have found that when the beating between the injected comb and the CW P1 dynamics generates frequencies harmonically related to the CW P1 oscillation frequency, a periodic comb can be achieved. It is important to note, however, that these results apply explicitly to the specific comb injection conditions used in our experiments (i.e. 3 comb lines with  $f_{mod} = 2 \text{ GHz}$  and  $V_{RF} = 150 \text{ mV}$ ) and might not hold for other conditions. We have also reported for the first time a polarization-resolved

**Table A.1**  
Description of the abbreviated terms.

Abbreviation	Description
OFC	Optical Frequency Comb
$\Delta f'$	Frequency comb spacing
DFB	Distributed Feedback Laser
DML	Discrete Mode laser
VCSEL	Vertical-Cavity Surface-Emitting Laser
MZM	Mach Zehnder modulator
ML	Mode-locking
GS	Gain-switching
RF	Radiofrequency
CW	Continuous Wave
$f_0$	CW P1 oscillation frequency
$f_{mod}$	Modulation frequency
$V_{RF}$	Modulation amplitude
GS-OFC	Gain-switched OFC
OI	Optical Injection
PS	Polarization Switching
FP	Fabry–Pérot
$P_{inj}$	Injected power
CNR	Carrier-to-noise ratio
$\Delta\nu$	Frequency detuning
IL	Injection Locking under CW OI
EPIL	Elliptically polarized injection locked state
P1	Period 1 under CW OI
P2	Period 2 under CW OI
IL'	Injection locking under OFC injection
PN'	OFC of Period N'
Modulated-EPIL	Modulated elliptically polarized injection locked state
ROF	Relaxation oscillation frequency
OC	Optical circulator
PC	Polarization controller
VOA	Variable optical attenuator
PM	Power meter
PBS	Polarization Beam Splitter
$I_{bias,DML/VCSEL}$	DC bias current applied to the DML or VCSEL
$I_{PS}$	Polarization switching current
$\lambda_{  }$	Dominant polarization emission wavelength of the free-running VCSEL
$I_{th,DML/VCSEL}$	Threshold current of the DML or VCSEL
$\nu_{  }$	Dominant polarization emission frequency of the free-running VCSEL
$\nu_{\perp}$	Suppressed polarization emission frequency of the free-running VCSEL
$\Delta\nu_1$	Frequency detuning under CW OI
$\Delta\nu_2$	Frequency detuning under OFC injection
$\nu_{inj}$	CW externally injected signal frequency
$\nu'_{inj}$	Central frequency of the injected comb

mapping of the P1 oscillation frequency and optical spectral width, obtained under CW OI, spanning both polarizations of the free-running VCSEL.

In conclusion, our work not only expands the existing knowledge about VCSEL's nonlinear dynamics under different OI conditions, but also offers fresh perspectives and avenues for the practical exploitation of these phenomena in a variety of fields. These include polarization-sensitive sensing, dual-comb ranging, and multicarrier optical sources for polarization division multiplexing optical communications. For these applications the stability is an important performance required for OFCs. The OFCs obtained in this work demonstrate negligible drift in comb lines' positions and intensities, highlighting the temporal stability. Our future work will focus on evaluating the phase noise of the generated combs. Further theoretical work using the Spin-Flip Model combined with Continuous-Wave and modulated optical injection similar to [38] will be undertaken to determine if our results can be generalized to other VCSEL types.

#### Declaration of competing interest

The authors declare that they have no known competing financial interests or personal relationships that could have appeared to influence the work reported in this paper.

#### Data availability

Data will be made available on request.

#### Acknowledgments

This research was supported by Fonds Wetenschappelijk Onderzoek (FWO), Belgium and by the Ministerio de Ciencia e Innovación (Spain), (PID2021-1234590B-C22MCIN/AEI/10.13039/501100011033/FEDER, UE.). D. Plaza-Vas and N. Vermeulen acknowledge financial support from FWO, Belgium under Grant G005420N and from VUB-OZR, Belgium. A. Quirce acknowledges financial support from Beatriz Galindo program, Ministerio de Ciencia, Innovación y Universidades (Spain).

#### Appendix. Table of abbreviations

See Table A.1.

#### References

- [1] T. Fortier, E. Baumann, 20 Years of developments in optical frequency comb technology and applications, *Commun. Phys.* 2 (153) (2019) 1–16, <http://dx.doi.org/10.1038/s42005-019-0249-y>.
- [2] M. Imran, P.M. Anandarajah, A. Kaszubowska-Anandarajah, N. Sambo, L. Poti, A survey of optical carrier generation techniques for terabit capacity elastic optical networks, *IEEE Commun. Surv. Tutor.* 20 (1) (2018) 211–263, <http://dx.doi.org/10.1109/COMST.2017.2775039>.
- [3] P. Trocha, M. Karpov, D. Ganin, M.H.P. Pfeiffer, A. Kordts, S. Wolf, J. Krockenberger, P. Marin-Palomo, C. Weimann, S. Randel, W. Freude, T.J. Kippenberg, C. Koos, Ultrafast optical ranging using microresonator soliton frequency combs, *Science* 359 (6378) (2018) 887–891, <http://dx.doi.org/10.1126/science.aao3924>.
- [4] N.R. Newbury, Searching for applications with a fine-tooth comb, *Nat. Photon.* 5 (2011) 186–188, <http://dx.doi.org/10.1038/nphoton.2011.38>.
- [5] P. Martín-Mateos, M. Ruiz-Llata, J. Posada-Roman, P. Acedo, Dual-comb architecture for fast spectroscopic measurements and spectral characterization, *IEEE Photonics Technol. Lett.* 27 (12) (2015) 1309–1312, <http://dx.doi.org/10.1109/LPT.2015.2421276>.
- [6] E. Prior, A.R. Criado, C.D. Dios, P. Acedo, M. Ortsiefer, P. Meissner, Continuous wave sub-THz photonic generation with vcsel-based optical frequency comb, *Electron. Lett.* 49 (15) (2013) 944–945, <http://dx.doi.org/10.1049/el.2013.1896>.
- [7] P.M. Anandarajah, S.P.O. Dúill, R. Zhou, L.P. Barry, Enhanced optical comb generation by gain-switching a single-mode semiconductor laser close to its relaxation oscillation frequency, *IEEE J. Sel. Top. Quantum Electron.* 21 (6) (2015) 592–600, <http://dx.doi.org/10.1109/JSTQE.2015.2456751>.
- [8] H.-F. Liu, W.F. Ngai, Nonlinear dynamics of a directly modulated 1.55  $\mu\text{m}$  InGaAsP distributed feedback semiconductor laser, *IEEE J. Quantum Electron.* 29 (6) (1993) 1668–1675, <http://dx.doi.org/10.1109/3.234419>.
- [9] P.M. Anandarajah, R. Maher, Y.Q. Xu, S. Latkowski, J. O'Carroll, S.G. Murdoch, R. Phelan, J. O'Gorman, L.P. Barry, Generation of coherent multicarrier signals by gain switching of discrete mode lasers, *IEEE Photonics J.* 3 (1) (2011) 112–122, <http://dx.doi.org/10.1109/JPHOT.2011.2105861>.
- [10] E. Prior, C.D. Dios, M. Ortsiefer, P. Meissner, P. Acedo, Understanding vcsel-based gain switching optical frequency combs: Experimental study of polarization dynamics, *J. Lightwave Technol.* 33 (22) (2015) 4572–4579, <http://dx.doi.org/10.1109/JLT.2015.2476956>.
- [11] F. Koyama, Recent advances of vcsel photonics, *J. Lightwave Technol.* 24 (12) (2006) 4502–4513, <http://dx.doi.org/10.1109/JLT.2006.886064>.
- [12] R. Michalzik, VCSELs Fundamentals, Technology and Applications of Vertical-Cavity Surface-Emitting Lasers, in: Springer Series in Optical Sciences, vol. 166, 2013, <http://dx.doi.org/10.1007/978-3-642-24986-0>.
- [13] V. Torres-Company, A.M. Weiner, Optical frequency comb technology for ultra-broadband radio-frequency photonics, *Laser Photon. Rev.* 8 (3) (2014) 368–393, <http://dx.doi.org/10.1002/lpor.201300126>.
- [14] Y. Doumbia, D. Wolfersberger, K. Panajotov, M. Sciamanna, Tailoring frequency combs through vcsel polarization dynamics, *Opt. Express* 29 (21) (2021) 33976–33991, <http://dx.doi.org/10.1364/oe.432281>.
- [15] Y. Doumbia, T. Malica, D. Wolfersberger, K. Panajotov, M. Sciamanna, Nonlinear dynamics of a laser diode with an injection of an optical frequency comb, *Opt. Express* 28 (21) (2020) 30379–30390, <http://dx.doi.org/10.1364/oe.402120>.
- [16] J. Davila-Rodriguez, K. Bagnell, P.J. Delfyett, Frequency stability of a 10 ghz optical frequency comb from a semiconductor-based mode-locked laser with an intracavity 10,000 finesse etalon, *Opt. Lett.* 38 (18) (2013) 3665–3668, <http://dx.doi.org/10.1364/ol.38.003665>.
- [17] A. Rosado, A. Pérez-Serrano, J.M.G. Tijero, A. Valle, L. Pesquera, I. Esquivias, Enhanced optical frequency comb generation by pulsed gain-switching of optically injected semiconductor lasers, *Opt. Express* 27 (6) (2019) 9155–9163, <http://dx.doi.org/10.1364/oe.27.009155>.

- [18] S.P. O'duill, P.M. Anandarajah, R. Zhou, L.P. Barry, Numerical investigation into the injection-locking phenomena of gain switched lasers for optical frequency comb generation, *Appl. Phys. Lett.* 106 (211105) (2015) 1–6, <http://dx.doi.org/10.1063/1.4921852>.
- [19] A. Rosado, A. Pérez-Serrano, J.M.G. Tijero, Ángel Valle, L. Pesquera, I. Esquivias, Experimental study of optical frequency comb generation in gain-switched semiconductor lasers, *Opt. Laser Technol.* 108 (2018) 542–550, <http://dx.doi.org/10.1016/j.optlastec.2018.07.038>.
- [20] A. Rosado, A. Pérez-Serrano, J.M.G. Tijero, A.V. Gutierrez, L. Pesquera, I. Esquivias, Numerical and experimental analysis of optical frequency comb generation in gain-switched semiconductor lasers, *IEEE J. Quantum Electron.* 55 (6) (2019) 1–12, <http://dx.doi.org/10.1109/JQE.2019.2943482>.
- [21] A.R.C. Serrano, C.D.D. Fernandez, E.P. Cano, M. Ortsiefer, P. Meissner, P. Acedo, Vcsel-based optical frequency combs: Toward efficient single-device comb generation, *IEEE Photonics Technol. Lett.* 25 (20) (2013) 1981–1984, <http://dx.doi.org/10.1109/LPT.2013.2280700>.
- [22] A. Quirce, C.D. Dios, A. Valle, L. Pesquera, P. Acedo, Polarization dynamics in vcsel-based gain switching optical frequency combs, *J. Lightwave Technol.* 36 (10) (2018) 1798–1806, <http://dx.doi.org/10.1109/JLT.2018.2790435>.
- [23] C.H. Chang, L. Chrostowski, C.J. Chang-Hasnain, Injection locking of vcsels, *IEEE J. Sel. Top. Quantum Electron.* 9 (5) (2003) 1386–1393, <http://dx.doi.org/10.1109/JSTQE.2003.819510>.
- [24] K. Panajotov, I. Gatare, A. Valle, H. Thienpont, M. Sciamanna, Polarization- and transverse-mode dynamics in optically injected and gain-switched vertical-cavity surface-emitting lasers, *IEEE J. Quantum Electron.* 45 (11) (2009) 1473–1481, <http://dx.doi.org/10.1109/JQE.2009.2024958>.
- [25] I. Gatare, J. Buesa, H. Thienpont, K. Panajotov, M. Sciamanna, Polarization switching bistability and dynamics in vertical-cavity surface-emitting laser under orthogonal optical injection, *Opt. Quantum Electron.* 38 (2006) 429–443, <http://dx.doi.org/10.1007/s11082-006-0041-6>.
- [26] J.B. Altés, I. Gatare, K. Panajotov, H. Thienpont, M. Sciamanna, Mapping of the dynamics induced by orthogonal optical injection in vertical-cavity surface-emitting lasers, *IEEE J. Quantum Electron.* 42 (2) (2006) 198–207, <http://dx.doi.org/10.1109/JQE.2005.862025>.
- [27] R. Al-Seyab, K. Schires, N.A. Khan, A. Hurtado, I.D. Henning, M.J. Adams, Dynamics of polarized optical injection in 1550-nm vcsels: Theory and experiments, *IEEE J. Sel. Top. Quantum Electron.* 17 (5) (2011) 1242–1249, <http://dx.doi.org/10.1109/JSTQE.2011.2138683>.
- [28] A. Quirce, P. Pérez, A. Valle, L. Pesquera, Correlation properties and time-resolved dynamics of linear polarizations emitted by single-mode vertical-cavity surface-emitting lasers subject to orthogonal optical injection, *J. Opt. Soc. Amer. B* 28 (11) (2011) 2765–2776, <http://dx.doi.org/10.1364/JOSAB.28.002765>.
- [29] J.P. Toomey, C. Nickkawde, D.M. Kane, K. Schires, I.D. Henning, A. Hurtado, M.J. Adams, Stability of the nonlinear dynamics of an optically injected vcsel, *Opt. Express* 20 (9) (2012) 10256–10270, <http://dx.doi.org/10.1364/OE.20.101256>.
- [30] A. Quirce, P. Perez, H. Lin, A. Valle, L. Pesquera, K. Panajotov, H. Thienpont, Polarization switching regions of optically injected long-wavelength vcsels, *IEEE J. Quantum Electron.* 50 (11) (2014) 921–928, <http://dx.doi.org/10.1109/JQE.2014.2360236>.
- [31] M. Torre, A. Hurtado, A. Quirce, A. Valle, L. Pesquera, M. Adams, Polarization switching in long-wavelength vcsels subject to orthogonal optical injection, *IEEE J. Quantum Electron.* 47 (1) (2011) 92–99, <http://dx.doi.org/10.1109/JQE.2010.2061219>.
- [32] M. Sciamanna, K. Panajotov, Route to polarization switching induced by optical injection in vertical-cavity surface-emitting lasers, *Phys. Rev. A* 73 (2006) 023811, <http://dx.doi.org/10.1103/PhysRevA.73.023811>.
- [33] M. AlMulla, Microwave frequency comb generation through optical double-locked semiconductor lasers, *Optik* 223 (2020) 165506, <http://dx.doi.org/10.1016/j.ijleo.2020.165506>.
- [34] B. Lingnau, K. Shortiss, F. Dubois, F.H. Peters, B. Kelleher, Universal generation of devil's staircases near hopf bifurcations via modulated forcing of nonlinear systems, *Phys. Rev. E* 102 (3) (2020) 030201, <http://dx.doi.org/10.1103/PhysRevE.102.030201>.
- [35] K. Shortiss, B. Lingnau, F. Dubois, B. Kelleher, F.H. Peters, Harmonic frequency locking and tuning of comb frequency spacing through optical injection, *Opt. Express* 27 (25) (2019) 36976–36989, <http://dx.doi.org/10.1364/oe.27.036976>.
- [36] R. Desmet, M. Virte, Laser diodes with modulated optical injection: Towards a simple signal processing unit? *J. Phys. Photon.* 2 (2) (2020) 025002, <http://dx.doi.org/10.1088/2515-7647/ab7081>.
- [37] Y. Doumbia, T. Malica, D. Wolfersberger, K. Panajotov, M. Sciamanna, Optical injection dynamics of frequency combs, *Opt. Lett.* 45 (2) (2020) 435–438, <http://dx.doi.org/10.1364/ol.381039>.
- [38] Y. Doumbia, D. Wolfersberger, K. Panajotov, M. Sciamanna, Two polarization comb dynamics in vcsels subject to optical injection, *Photonics* 9 (2) (2022) 115, <http://dx.doi.org/10.3390/photonics9020115>.
- [39] H. Lin, P. Pérez, A. Valle, L. Pesquera, Investigation of elliptically polarized injection locked states in vcsels subject to orthogonal optical injection, *Opt. Express* 22 (5) (2014) 4880–4885, <http://dx.doi.org/10.1364/oe.22.004880>.
- [40] G. Jain, D. Gutierrez-Pascual, M. Wallace, J. Donegan, P. Anandarajah, Experimental investigation of external optical injection and its application in gain-switched wavelength tunable optical frequency comb generation, *J. Lightwave Technol.* 39 (18) (2021) 5884–5895, <http://dx.doi.org/10.1109/JLT.2021.3091956>.
- [41] K.H. Jeong, K.H. Kim, S.H. Lee, M.H. Lee, B.S. Yoo, K.A. Shore, Optical injection-induced polarization switching dynamics in 1.5  $\mu\text{m}$  wavelength single-mode vertical-cavity surface-emitting lasers, *IEEE Photonics Technol. Lett.* 20 (10) (2008) 779–781, <http://dx.doi.org/10.1109/LPT.2008.921110>.